Longitudinal Finger Rotation—Deformation Detection and Correction

Bernhard Prommegger, Christof Kauba, Michael Linortner, and Andreas Uhl

***Abstract*—Finger vein biometrics is becoming more and more popular. However, longitudinal finger rotation, which can easily occur in practical applications, causes severe problems as the resulting vein structure is deformed in a non-linear way. These problems will become even more important in the future, as finger vein scanners are evolving toward contact-less acquisition. This paper provides a systematic evaluation regarding the influence of longitudinal rotation on the performance of finger vein recognition systems and the degree to which the deformations can be corrected. It presents two novel approaches to correct the longitudinal rotation, one based on the known rotation angle. The second one compensates the rotational deformation by applying a rotation correction in both directions using a pre-defined angle combined with score level fusion and works without any knowledge of the actual rotation angle. During the experiments, the aforementioned approaches and two additional are applied: one correcting the deformations based on an analysis of the geometric shape of the finger and the second one applying an elliptic pattern normalization of the region of interest. The experimental results confirm the negative impact of longitudinal rotation on the recognition performance and prove that its correction noticeably improves the performance again.**

***Index Terms*—Finger vein recognition, longitudinal finger rotation, finger rotation detection, finger rotation correction, biometric fusion.**

I. Introduction

VASCULAR pattern based biometric systems, commonly denoted as vein biometrics, offer several advantages over other well-established biometric recognition systems. In particular, hand and finger vein systems have become a serious alternative to fingerprint based ones for several applications. Vein based systems use the structure of the blood vessels inside the human body, which becomes visible under near-infrared (NIR) light. As the vein structure is located inside the human body, it is resistant to abrasion and external influences on the skin. Furthermore, a lifeness detection to detect presentation attacks can be performed easily [1].

Manuscript received September 10, 2018; revised January 15, 2019; accepted February 14, 2019. Date of publication March 7, 2019; date of current version April 19, 2019. This work was supported in part by the European Union's Horizon 2020 Research and Innovation Program under Grant 700259, and in part by the FFG KIRAS Project AUTFingerATM under Grant 864785. This paper was recommended for publication by Associate Editor D. Maio upon evaluation of the reviewers' comments. *(Corresponding author: Bernhard Prommegger.)*

The authors are with the Department of Computer Sciences, University of Salzburg, 5020 Salzburg, Austria (e-mail: bprommeg@cs.sbg.ac.at; ckauba@cs.sbg.ac.at; mlinortner@cs.sbg.ac.at; uhl@cs.sbg.ac.at).

Digital Object Identifier 10.1109/TBIOM.2019.2902020

The performance of finger vein recognition systems suffers from different internal and external factors. Internal factors include the design and configuration of the sensor itself, especially the NIR light source and the camera module. External factors include environmental conditions (e.g., temperature and humidity) and deformations due to misplacement of the finger, typically including shifts, tilt, bending and longitudinal rotation which will be further examined in this work.

Performance degradations caused by various types of finger misplacement are not new and have been addressed in several publications. The need for a robust finger vein image normalisation including rotational alignment has already been mentioned by Kumar and Zhou in 2012 [1]. Chen *et al.* [2] state that deformation correction can be done either during pre-processing, feature extraction or comparison. Moreover, the physical design of the sensor can help to avoid misplacements of the finger. Prommegger *et al.* [3] showed, that longitudinal finger rotation has a severe influence on the recognition performance of a finger vein recognition system. There are several approaches that try to reduce the influence of these issues during the processing of the vein patterns. Kumar and Zhou [1] introduced a finger alignment based on the finger boundary to overcome finger translation and rotation. Lee *et al.* [4] proposed a system utilizing a minutia based alignment together with local binary patterns as feature extraction method. Huang *et al.* [5] improved the resistance against longitudinal rotation by applying an elliptic pattern normalization to the input images. Matsuda *et al.* [6] proposed a feature-point based recognition system introducing a finger-shape model and a non-rigid registration method. They achieved robustness against longitudinal rotation up to $\pm 30°$. Yang *et al.* [7] introduced a finger vein recognition framework including an anatomy structure analysis based vein extraction algorithm and integration matching strategy. Chen *et al.* [2] introduced an approach that detects different types of finger deformation by analysing the shape of the finger, e.g., around the longitudinal axis, and corrects them using linear and non-linear transformations. Besides these software based solutions, there are some hardware-based ones which aim to prevent finger misplacements in the first place, during acquisition, rather than correcting them afterwards. Kauba *et al.* [8] presented a finger vein scanner that captures three fingers at once and requires the subject to place the fingers in a flat, aligned position on a finger shaped guiding surface. This reduces longitudinal finger rotation, planar finger rotation as well as finger shifts to a minimum. To the best of our knowledge, there is no method that satisfactory solves the problem

of longitudinal finger rotation. Problems resulting from finger misplacements, e.g., longitudinal rotation, will receive more attention in the future as finger vein systems evolve towards contact-less operation.

The main contribution of our work is the systematic analysis to which extent a longitudinal finger rotation can be compensated and which impact such a correction has on the recognition accuracy of the finger vein recognition system. This analysis extends the authors previous work [3], [9]. Therefore, we evaluate four different methods to correct the longitudinal rotaion, where the first and the last on are proposed in this work:

1) A correction using the actual rotation angle provided by the data set and a circular projective correction. This approach has not been applied in finger vein recognition and serves as a reference for the effectiveness of the other rotation compensation methods.
2) A method proposed by Chen *et al.* [2] that analyses the geometric shape of the finger and corrects the deformations based on the results.
3) Elliptic pattern normalization of the region of interest as proposed by Huang *et al.* [5].
4) A new method proposed in this article that compensates the rotational deformations without the knowledge of the actual rotation angle by applying a rotation correction in both directions using a pre-defined angle combined with score level fusion.

To verify the effectiveness of the proposed approach (4), it is also applied on two commonly used finger vein data sets, namely UTFVP [10] and SDUMLA-HMT [11].

The rest of this paper is organized as follows: Longitudinal finger rotation and its problems caused for finger vein recognition systems are described in more detail in Section II. Section III explains all details of the used rotation compensation methods. Section IV explains the processing tool-chain and the used data set together with the experimental set-up. Furthermore it includes the experimental results together with a discussion. Section V concludes the paper along with an outlook on future work.

II. Longitudinal Finger Rotation

While capturing finger vein images, the finger's placement on the scanner is not necessarily done in an optimal way. Such misplacements result in deformations of the vein structure, affecting the performance of a finger vein recognition system. Fig. 1 shows the orientations of the x, y and z axis with respect to the finger. The different types of misplacements include:

- shifts of the finger in x- and y-direction (planar shifts)
- shifts of the finger in z-direction (distance to the camera, scaling)
- planar rotation of the finger (in the xy-plane)
- tilts of the finger (finger tip and finger root are not in the same xy-plane)
- finger bending and
- rotation around the longitudinal axis of the finger (y-axis).

As described in the authors' previous work [3], some of the problematic misplacements can be reduced or even completely

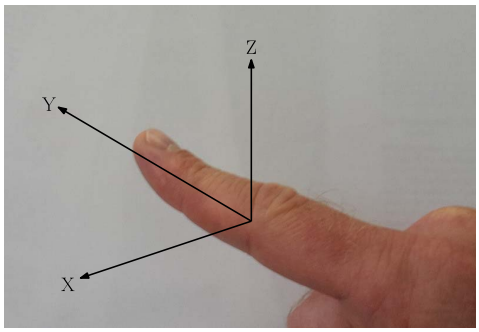

Fig. 1. Definition of the axes of a finger in a three-dimensional space.

Fig. 2. Finger rotation example using a commercial off-the-shelf scanner (rotation counter-clockwise, originally published in [3]).

prevented during acquisition by adding simple support structures on the scanner, e.g., guiding walls to prevent planar shifts. Moreover, they can be corrected by the biometric processing chain during pre-processing (finger alignment during ROI extraction) or feature extraction and comparison (using x- and y-direction shifted and rotated versions of the extracted templates). Almost all currently available commercial off-the-shelf (COTS) sensors are equipped with such support structures, but most of them are still not able to prevent a rotation around the y-axis (longitudinal finger rotation). Thus, longitudinal finger rotation cannot be ruled out and poses a severe problem to finger vein recognition systems. Fig. 2 shows an example of the longitudinal finger rotation while using a COTS scanner. In a supervised acquisition scenario, the user can be guided to place the finger correctly. However, in unsupervised operation of the scanner, such longitudinal rotations are highly likely to occur. As finger vein scanner development tends towards contact-less operation, the problem of finger misplacement is getting more serious due the increased degrees of freedom and the inability to use guiding structures.

The captured vein structure is a projection of the vessel structure in the 3D space onto a 2D plane. If the finger is rotated along its longitudinal axis, the vein pattern is deformed according to a non-linear transformation. Fig. 3. shows the effect of longitudinal finger rotation on the vein pattern. The finger cross section (top row) is rotated from $-30°$ to $+30°$. As a result of this rotation, the projected pattern of the veins (bottom row) changes as well. Depending on the relative position of the veins to each other and the rotation angle, some of the captured veins might merge into a single one. The vein structures of $-30°$ (left), $0°$ (middle) and $30°$ (right) are completely

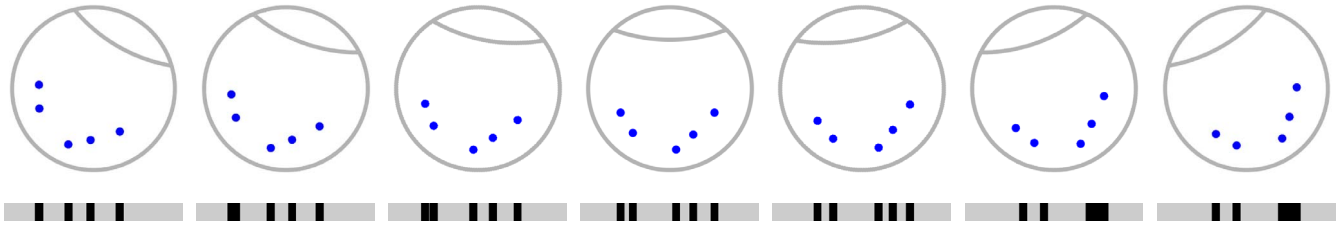

Fig. 3. Longtitudinal finger rotation principle: A schematic finger cross section showing five veins (blue dots) rotated from −30° (left) to +30° (right) in 10° steps. The projection (bottom row) of the vein pattern is different according to the rotation angle following a non-linear transformation (originally published in [3]).

different. Widely used vein recognition schemes can handle such deformations only to a certain extent [3]. If the deformations caused by the longitudinal rotation are corrected, the negative impact can be reduced, but not completely mitigated.

III. Finger Rotation Compensation

As longitudinal finger rotation decreases the performance of a finger vein recognition system, it is beneficial to compensate the deformations caused by this rotation. In this study, four different approaches to tackle this problem are discussed and analysed. The first approach which has not been applied in finger vein recognition sp far assumes that the longitudinal rotation angle is known and compensates the deformation by applying a non-linear transformation in the opposite direction. This kind of analysis was only possible because the *PLUSVein Finger Rotation data set* (PLUSVein-FR) provides the actual angle of the longitudinal finger rotation. The results of this method can be used as a reference for the evaluation of the effectiveness of the other rotation correction methods as the results of this method will be close to the possible best achievable results. The second approach, proposed by Chen *et al.* [2], tries to detect the finger rotation by analysing the finger shape and again correcting it using a non-linear transformation. The third method applies an elliptic pattern normalization (EPN) [5] of the acquired image to reduce the deformations. The last approach is a novel approach proposed by the authors. It applies a rotation compensation in both directions using a fixed angle together with a maximum rule score level fusion. Its main advantage is that no prior knowledge of the actual rotation angle is required.

A. Rotation Compensation for Known Rotation Angle

For an accurate correction of the vein pattern the position of the veins in the 2D image as well as the shape of the finger and the depth of the veins within the finger has to be known. As this information is not available in general, both need to be estimated. We approximate the shape of the finger as a circle like Matsuda *et al.* did in [6]. We further assume, that the veins are located on the skin surface instead of underneath the skin. Therefore, the vein pattern is projected back on the outer circle of the finger. Fig. 4 depicts this principle. The left image shows a schematic cross section of a finger acquired with a longitudinal rotation $\varphi_{rotate} = 25°$. The blue dots represent the veins in their proper position, the red ones those that are projected onto the skin. The bar below is a visualization of the

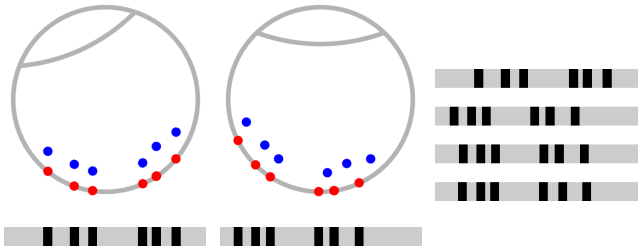

Fig. 4. Principle of rotation correction with known rotation angle. Left: finger rotated with 25°. The blue points depict the veins inside the finger, the red points the veins projected on the finger shape. The bar below is the projected vein pattern. Middle: the finger rotated into the palmar view. The bar below is the rotation corrected vein pattern, which corresponds to the veins estimated on the finger surface. On the right side the vein patterns are visualized below each other. From top to bottom: rotated vein pattern, corrected vein pattern, corrected pattern shifted for the highest correlation to the palmar pattern (bottom row).

vein pattern, where the black areas correspond to the veins. In the middle image, the finger is rotated back into the ideal palmar position ($\varphi_{rotate} = 0°$). It is clearly visible that the blue and red dots are not perfectly aligned with each other. From top to bottom, the right side shows the vein patterns of the acquired image (same as on the left side), the rotated pattern (same as in the middle), a shifted version of the rotated pattern and the original pattern that would have been acquired without the presence of longitudinal rotation. The rotation corrected pattern is clearly more similar to the original pattern than the acquired one. The additional shift is applied to achieve a higher correlation between the corrected patterns and the original one.

The position of a pixel within the vein pattern is defined by its x-coordinate x_r and the corresponding y-coordinate y_r, which is calculated by (1)

$$y_r = \sqrt{r^2 - x_r^2} \tag{1}$$

where r is the approximated radius of the finger. r is half the finger width, which corresponds to half of the height of the extracted finger ROI. The rotation back into the palmar view is calculated by applying the rotation matrix given in (2).

$$\begin{bmatrix} x_p \\ y_p \end{bmatrix} = \begin{bmatrix} cos(-\varphi_{rotate}) & -sin(-\varphi_{rotate}) \\ sin(-\varphi_{rotate}) & cos(-\varphi_{rotate}) \end{bmatrix} * \begin{bmatrix} x_r \\ y_r \end{bmatrix} \tag{2}$$

x_p and y_p are the corrected coordinates of the vein pixel in the palmar view and φ_{rotate} is the rotation angle. If the veins are located on the skin surface and the finger radius is known exactly, this method is accurate. In practice, the blood vessels

are inside the finger and the finger outline detection my not be completely accurate, thus there remains a small deviation.

B. Geometric Shape Analysis Based Finger Rotation Deformation Detection and Correction

Chen *et al.* [2] proposed a method to detect and correct finger deformations based on a geometric shape analysis (GADC). They distinguished three types of finger deformations: finger tilt, finger bending and longitudinal finger rotation. In this work only longitudinal finger rotation, which Chen *et al.* called a type 3 deformation, is discussed. For the shape analysis they defined several parameters, on the basis of which they calculated statistical measures of the finger. These parameters are described in Section II of the original paper. The detection of a type 3 deformation is based on the bending at the proximal inter-phalangeal joint. If the absolute difference of the upper and lower angle of the finger outline at the joint, α_{upp_joint1} and α_{down_joint1}, is larger than a defined threshold $t_{3rotate}$, a deformation of type 3 is present and the image has to be corrected. The rotation correction is applied either in the one or the other direction using a fixed sampling scheme. Thus, the same fixed correction is applied independent of the actual rotation angle. A detailed description of the rotation detection and correction scheme can be found in [2].

C. Elliptic Pattern Normalization

Huang *et al.* [5] proposed a normalization of the vein pattern in the feature space. The method is based on the hypothesis, that the cross section of a finger approximately resembles an ellipsis and that the veins which are captured by the finger vein scanner are located close to the finger surface. Their normalization essentially corresponds to a rolling of the finger, which reduces the non-linear deformation of the vein structure across the entire width of the finger. After this correction is applied, a horizontal shift of the images during comparison corresponds to a rotation of the finger. They applied the elliptic normalization in the feature space using a vein pattern based feature extraction. As this paper also investigates algorithms that are not vein pattern based, an elliptic correction in the feature space is not feasible for all of them. Therefore, the correction is applied in the image space. This way the normalization can be used for all algorithms under investigation. For more details on this method, the interested reader is referred to the original work [5].

D. Rotation Compensation Using a Fixed Angle

In real world scenarios, the longitudinal rotation angle is unknown and its estimation is a difficult task. Hence, a method that does not require the rotation angle to correct the images would be beneficial. As shown in [3], commonly used recognition schemes tolerate rotations of at least $\pm 10°$. Thus, a system that is able to keep the deformations caused by the longitudinal rotation within this range is desirable.

The proposed method for correcting longitudinal finger rotation is based on rotations of the image in both directions using a fixed compensation angle. The final score is calculated using a maximum rule score level fusion of the three comparisons (original, non-rotated image and the two rotated versions).

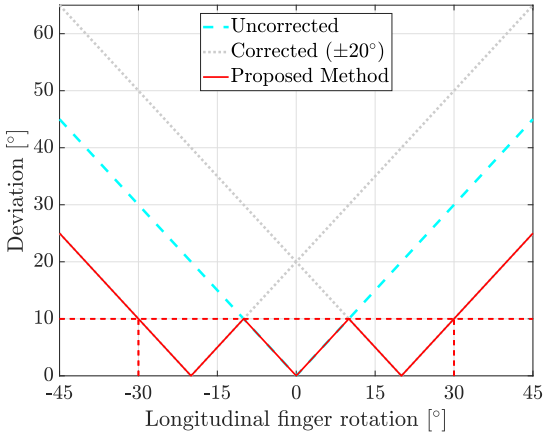

Fig. 5. Deviation of the rotated finger to the palmar view with an correction angle $\varphi_{corr} = 20°$.

It is assumed that the enrolment data is acquired in a constrained environment. Thus, the longitudinal rotation of the enrolment data should be close to 0°. During the image acquisition, the finger can be positioned either correctly (no rotation) or rotated to the left or to right side. In order to reduce the rotational deviation between the two samples, comparisons using the captured sample itself with respect to the unmodified enrolled sample and its rotated versions in both directions are applied. The angle of the applied rotation φ_{corr} is defined in advance. The applied rotation compensation is the same as explained in Section III-A: the finger is approximated as a circle and the image is projected on this circle prior to applying the rotation correction.

Fig. 5 illustrates how this approach reduces the rotational deviation with $\varphi_{corr} = 20°$. The dashed cyan line shows the deviation of the rotation for the original data. The dotted grey lines represent the deviation of the data corrected with $\pm\varphi_{corr}$. The red line corresponds to the minimum deviation of all images to the enrolled one. It can be seen that the rotational angle of the sample compared to the original deviation is reduced. For example, if the probe sample is rotated $\varphi = 30°$ from the enrolled sample, the following comparisons are done:

1) The probe sample against the unmodified enrolled sample: rotation angle between the compared images: 30°.
2) The probe sample against the enrolled image rotated with φ_{corr}: rotation angle of $-\varphi + \varphi_{corr} = -30° + 20° = 10°$.
3) The probe sample against the enrolled image rotated with $-\varphi_{corr}$: rotation angle of $-\varphi - \varphi_{corr} = -30° - 20° = 50°$.

If $\varphi_{corr} = 20°$, the deviation does not exceed 10° if the rotation angle stays within a range of $\pm 30°$. This deviation can be handled by commonly used recognition schemes and thus, the performance degradation can be kept at an acceptable level. The best choice for φ_{corr} depends on the actual application and the scanner device. The useful range of φ_{corr} is in the range of 5° to 25° for most applications.

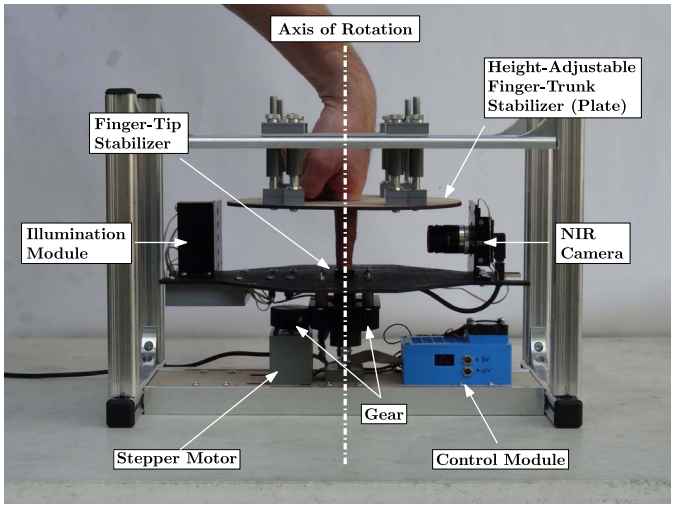

Fig. 6. Basic principle of the multi-perspective finger vein scanner used to acquire the *PLUSVein-FR* data set (originally published in [9], © 2018 IEEE).

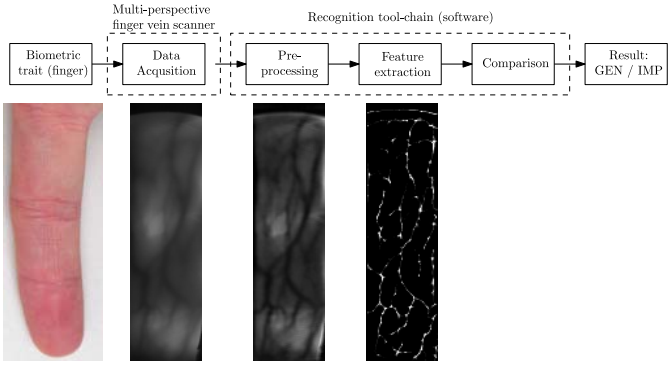

Fig. 7. Basic components of a biometric recognition system (originally published in [3]).

IV. Experiments

During the experiments, the four rotation compensation approaches described in Section III are applied on the *PLUSVein finger rotation data set*, which is described in the following subsection. Furthermore, to verify effectiveness of the proposed fixed angle method, it is applied on the publicly available finger vein data sets UTFVP [10] und SDUMLA-HMT [11].

A. PLUSVein Finger Rotation Data Set

The *PLUSVein Finger rotation data set* (PLUSVein-FR) has been acquired using a custom designed multi-perspective finger vein scanner as depicted in Fig. 6. It provides finger vein images all around the finger (360°) with a resolution of 1°. The finger is placed in the center of the scanner (axis of rotation), whereas the NIR camera (right side) and the NIR illumination unit (left side) are placed on opposite sides of the finger (light transmission). The different projections of the finger are acquired by rotating the camera and the illumination module around the finger.

The data set contains finger images captured from 63 different subjects, 4 fingers per subject, which sums up to a total of 252 unique fingers. Each finger is acquired 5 times. This results in 1.260 images per perspective. In this work, we use the perspectives in the range of ±45° around the palmar view in steps of 1°. For more details on the data set and the multi-perspective finger vein scanner, the interested reader is referred to the authors previous publications [3], [9]. The data set is publicly available for research purposes at http://wavelab.at/sources/PLUSVein-FingerRotationDataSet.

B. Recognition Tool-Chain

The components of the recognition tool-chain are visualized in Fig. 7, which are the same as in the authors previous work [9]: First, the biometric trait is acquired by the multi-perspective finger vein scanner as a video sequence. The subsequent tool-chain consists of pre-processing (ROI (region of interest) extraction and image enhancement), feature extraction and comparison. At first the frames corresponding to 1° steps are extracted from the video sequences. Afterwards each image is processed individually: the ROI is extracted and the finger outline is detected using an edge detection algorithm. Then a straight line is fitted to the center of the finger. Based on this line, the finger is aligned (rotated and vertically shifted) such that it is in horizontal position and the center line of the finger is in the middle of the image. The area outside of the finger lines is masked out (pixels set to black). Afterwards, the image is cut to a pre-defined length of 1100 pixels. The height of the finger is normalized to a height of 300 pixels throughout the whole length of the finger image. To avoid artifacts at the image borders, 10 pixels are cut off on each side. The resulting ROI has a size of 280×1080 pixels. Fig. 8 visualizes this process. The top image shows the finger with the center and finger lines, the bottom image shows the final ROI. Furthermore, to improve the visibility of the vein patterns **High Frequency Emphasis Filtering** (HFE) [12], **Circular Gabor Filter** (CGF) [13] and simple **CLAHE** (local histogram equalisation) [14] are used as pre-processing techniques. For more details on the pre-processing methods refer to [15]. This study compares four simple and one advanced vein pattern based feature extraction methods which is based on the analysis of the anatomy structure of the veins. **Maximum Curvature** (MC) [16], **Principal Curvature** (PC) [17], **Wide Line Detector** (WLD) [5] and **Gabor Filter** (GF) [1] aim to extract the vein pattern from the background resulting in a binary image, followed by a comparison of these binary images. Comparing the binary feature images is done using a correlation measure, calculated between the input images and in x- and y-direction shifted and rotated versions of the reference image. The more sophisticated vein pattern based method, **Finger Vein Recognition With Anatomy Structure Analysis** (ASAVE), proposed by Yang *et al.* [7], is a finger vein recognition framework which includes an anatomy structure analysis based vein extraction algorithm and an integration matching strategy. In addition, two keypoint based recognition schemes, a **SIFT** [15] based technique with additional keypoint filtering and **Deformation-Tolerant Feature-Point Matching** (DTFPM) proposed by Matsuda *et al.* [6] are evaluated.

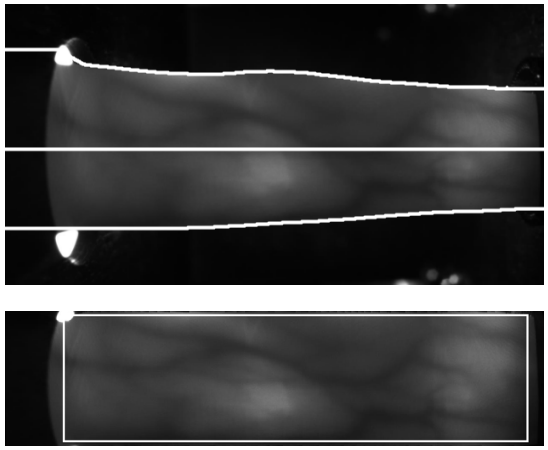

Fig. 8. ROI extraction - top: finger line detection. The straight line in the middle represents the center of the finger at which it is horizontally aligned. The top and bottom lines are the detected finger outlines which separate the finger from the background. The region between the lines is regarded as finger region. Bottom: the finger region is transformed to a fixed height. Afterwards the ROI, visualized as white square, of a fixed size is cut out.

TABLE I
NUMBER OF COMPARISONS FOR EACH SUBSETS

Name	Subjects	Genuine	Impostor	Total
Subset 1	32	3200	16384	19584
Subset 2	31	3100	15376	18476
Total	63	6300	31760	38060

C. Evaluation Protocol

To quantify the performance, the EER, the FMR100 (the lowest FNMR for FMR $\leq$ 1%), the FMR1000 (the lowest FNMR for FMR $\leq$ 0,1%) as well as the ZeroFMR (the lowest FNMR for FMR = 0%) are used. The data set is divided into two roughly equal sized subsets. The division is based on the contained subjects, i.e., all fingers of the same person are in one subset. Each subset is used to determine the parameters which are then applied to the other subset. This ensures a 100% separation of the data used for determining the optimal parameters and the actual test set. The evaluation within the subsets follows the test protocol of the FVC2004 [18]: for calculating the genuine scores, all possible genuine comparisons are performed. For calculating the impostor scores, only the first image of each finger is compared to the first image of all other fingers. The resulting number of comparisons for both subsets are listed in Table I. The final results are evaluated based on the combined scores (genuine and impostor) of both test runs. The parameter optimization is executed only for the original, unmodified data set. The same parameter settings are applied for all experiments on the modified versions of the data sets too.

To quantify the decrease in performance for the rotated finger vein images, the relative performance degradation (RPD), which is calculated as stated in equation (3), is used:

$$RPD = \frac{EER_x - EER_{ref}}{EER_{ref}}. \tag{3}$$

EER_{ref} is the EER of the reference data set and EER_x the EER of the evaluated data set. A RPD of 0 means no change in performance, a RPD of 1 corresponds to an EER increase to its doubled value. For a negative RPD, the performance increased. For the evaluation of the performance increase due to rotation correction, the relative performance increase (RPI) as in equation (4) is calculated:

$$RPI = \frac{EER_{ref} - EER_x}{EER_x}. \tag{4}$$

Again, EER_{ref} is the EER of the reference data set and EER_x the EER of the evaluated data set. A RPI of 0 means no change in the performance, a RPI of 1 corresponds to a drop in the EER to half of its value. For a negative RPI, the performance decreased. All values are given in percentage terms, e.g., 2.35 means 2.35%.

An implementation of the complete tool-chain as well as the used configuration files and results (EER, FMR100, FMR1000 and ZeroFMR) are available for download at: http://www.wavelab.at/sources/Prommegger19a.

TABLE II
BASELINE PERFORMANCE RESULTS AT THE PALMAR VIEW FOR THE DIFFERENT RECOGNITION SCHEMES ORDERED BY RECOGNITION PERFORMANCE

Feature	EER	FMR100	FMR1000	ZeroFMR
MC	0.37 ($\pm$0.09)	0.30	0.43	0.84
PC	0.77 ($\pm$0.13)	0.70	1.37	1.92
DTFPM	0.87 ($\pm$0.14)	0.83	2.27	6.85
WLD	0.92 ($\pm$0.14)	0.92	1.29	2.80
GF	1.02 ($\pm$0.15)	1.02	1.70	2.61
SIFT	1.80 ($\pm$0.20)	2.05	4.10	6.97
ASAVE	2.96 ($\pm$0.25)	3.91	5.74	15.07

D. Baseline Results

In order to quantify the change of the recognition performance due to rotation correction, the results of the unmodified PLUSVein-FR are calculated. In finger vein recognition usually the palmar perspective is used [10], [11], [19]–[22]. The performance of the data set achieved at this view is stated in Table II. The results are comparable to other publicly available finger vein data sets: MC achieves the best recognition rate with an EER of 0.37%, followed by PC, DTFPM, WLD, GF and SIFT while ASAVE, with an EER of 2.96%, performs worst.

The images captured at the different rotation angles from $-45°$ to $45°$ are compared to the palmar view (no rotation, $0°$). The trend of the absolute EER is shown in Fig. 9. MC, PC and WLD follow the same trend: They start at an EER $< 1\%$ and keep quite a stable performance up to $\pm 15°$, where their EER is still $< 1.5\%$. Higher rotations lead to a fast drop of the performance. At a rotation of $\pm 45°$, their EER is $> 40\%$. The trend of GF, the fourth of the simple vein pattern based methods, is similar, but its performance degradation is more prominent. Both keypoint based methods are more robust against longitudinal rotation. DTFPM shows the overall best performance and outperforms all vein pattern based methods for rotation angles higher than $\pm 30°$. At $\pm 45°$ its EER is still $< 20\%$. SIFT outperforms the other methods starting at $\pm 35°$ and achieves an EER of $< 30\%$ at $\pm 45°$. The more sophisticated ASAVE framework shows no advantage over the simple vein pattern based methods: It starts at a higher baseline EER

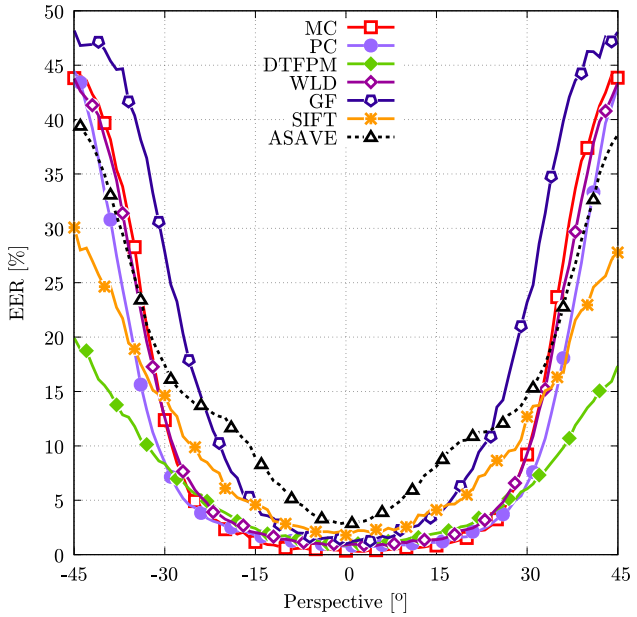

Fig. 9. Trend of the EER across the different rotation angles (0° corresponds to the palmar view) for the original, unmodified data set from −45° to 45°.

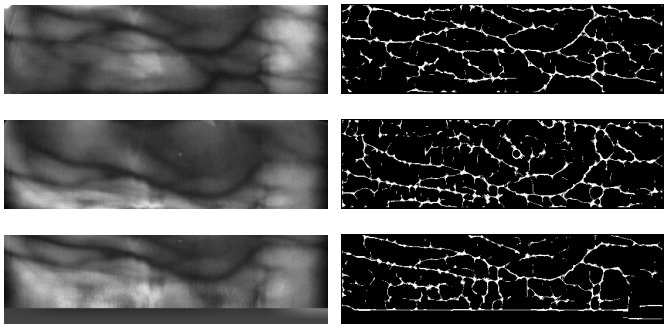

Fig. 10. ROI (left) and extracted MC features (right) of sample images of the PLUSVein-FR. First row: palmar view (0°), second row: 25° rotated view, bottom row: rotation corrected version of the 25° rotated image.

of 3% and its performance degrades towards higher rotation angles too, arriving at an EER of about 40% at ±45° as well.

As already shown in [3], all recognition schemes are able to tolerate a longitudinal finger rotation up to ±10°, while still achieving an acceptable performance. The EER values as well as the RPD for selected perspectives are stated in Table III. This table lists the performance indicators for all applied rotation correction methods and recognition schemes. The RPD is always calculated with respect to the palmar view (0°) of the same recognition scheme and rotation correction method. This allows a direct comparison of the different methods. Since the recognition results for rotations in both directions are almost symmetrical, the table only contains values for positive rotation angles.

E. Rotation Compensation for Known Rotation Angle

As mentioned in Section IV-A, for the PLUSVein-FR the exact angle of the longitudinal finger rotation is known. This fact can be exploited to apply an actual correction of the longitudinal finger rotation as described in Section III-A. Fig. 10

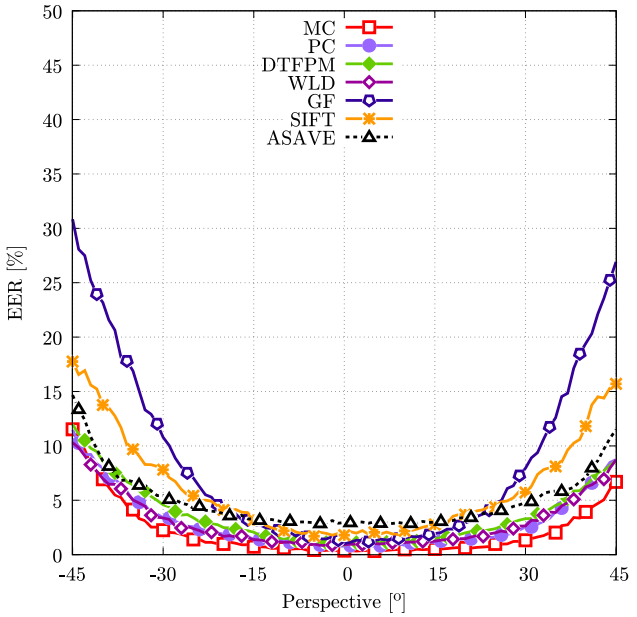

Fig. 11. Trend of the EER across the different rotation angles applying an exact longitudinal finger rotation compensation (0° corresponds to the reference, palmar view) from −45° to 45°.

depicts the ROI (left side) and the extracted MC features (right side) for different views. The images in the top row are from the palmar view, the middle shows the ones from a 25° rotated finger and the bottom row its corrected version. It is clearly visible that the vein structure of the rotated image (middle row) is a deformed version of the palmar one (top row). The vein structures of the rotation corrected images in the bottom row are more similar to the palmar images than the uncorrected ones. The part of the corrected ROI image that contains no information (due to the transform) is filled with the average grey level of the image.

Fig. 11 depicts the trend of the EER for the corrected images. For all methods, the drop in the recognition performance is less pronounced than without rotation compensation. Again, MC, PC and WLD show a similar trend: Up to a rotation angle of ±30° the EER stays below 3%. Even for a rotation of ±45° their EER is still below 9%. The performance of keypoint based algorithms increases as well, but not to the same extent as for MC, PC and WLD. These algorithms are already tolerant against longitudinal rotation, and thus, the potential for improvement due to rotation correction is smaller. Neither DTFPM, nor SIFT outperform the three simple vein pattern based methods. ASAVE benefits most from this correction: With a maximum RPD of $< 300\%$ over the whole range of ±45°, it exhibits the lowest performance degradation. Although, due to its low baseline performance, all methods except SIFT and GF still outperform ASAVE in terms of absolute EER. Again, GF shows the fastest performance degradation among all algorithms. These results indicate, that especially simple vein pattern based methods get the most out of the longitudinal rotation compensation. They are even able to outperform more sophisticated methods like DTFPM. Keypoint based methods, which are robust against rotation to some level, do only benefit from the correction to a small extent.

TABLE III
PERFORMANCE RESULTS IN TERMS OF EER AND RPD OF ALL CORRECTION METHODS AND RECOGNITION SCHEMES. THE RPD IS ALWAYS CALCULATED WITH RESPECT TO THE PALMAR VIEW (0°) OF THE SAME RECOGNITION SCHEME AND ROTATION CORRECTION METHOD. THE HIGHLIGHTED RESULTS (BOLD FACE) REPRESENT THE BEST RECOGNITION RATES FOR A RECOGNITION SCHEME AT THE SPECIFIED ROTATION ANGLE

Method	Rotation angle	No Correction		Known Angle		GADC		EPN		Fixed Angle		Fixed Angle + EPN	
		EER	RPD	EER	RPD	EER	RPD	EER	RPD	EER	RPD	EER	RPD
MC	0°	0.37	—	0.37	—	0.59	—	**0.17**	—	0.28	—	0.21	—
	5°	0.41	13.15	0.34	-8.26	0.81	37.29	0.17	0.97	0.30	6.18	**0.16**	-23.26
	10°	0.63	73.37	0.49	34.51	0.96	62.32	0.25	47.24	0.32	12.37	**0.19**	-7.75
	15°	0.84	130.68	0.52	42.86	1.11	86.94	**0.32**	84.36	0.38	33.71	0.34	62.80
	20°	1.54	320.82	0.62	68.94	2.05	246.62	0.67	286.94	0.62	117.99	**0.44**	115.50
	25°	3.25	788.35	0.99	169.35	4.42	646.06	1.13	555.40	1.00	252.26	**0.75**	262.02
	30°	9.21	2415.79	1.32	260.14	11.66	1866.52	1.99	1051.57	1.46	413.50	**1.05**	407.75
	35°	23.68	6372.16	2.03	453.54	25.21	4152.94	4.61	2570.63	2.55	798.34	**1.74**	746.51
	40°	37.39	10119.38	3.93	974.29	37.85	6284.78	10.88	6205.09	5.19	1724.77	**2.88**	1296.93
	45°	43.84	11882.56	6.69	1728.68	43.51	7239.77	25.19	14500.85	9.66	3299.00	**4.62**	2145.00
PC	0°	0.77	—	0.77	—	0.86	—	0.51	—	0.65	—	**0.46**	—
	5°	0.75	-2.67	0.76	-0.59	0.78	-9.23	0.51	0.04	0.65	0.00	**0.43**	-6.94
	10°	0.89	15.81	0.87	13.73	0.98	14.36	0.49	-3.45	0.92	41.17	**0.41**	-10.42
	15°	1.13	47.05	1.11	44.97	1.26	46.40	0.52	3.19	0.97	48.53	**0.46**	0.00
	20°	1.65	114.89	1.48	92.45	1.81	110.97	0.81	59.38	1.34	105.15	**0.63**	37.50
	25°	3.26	324.80	1.62	111.15	3.84	346.83	1.21	137.66	1.70	161.28	**0.86**	87.16
	30°	6.52	748.56	2.56	232.94	8.37	873.41	1.94	281.33	2.44	274.26	**1.16**	152.09
	35°	15.36	1897.84	3.93	411.87	17.91	1983.44	3.67	623.05	3.79	481.61	**1.78**	286.81
	40°	30.37	3851.08	6.06	688.84	31.64	3580.94	9.13	1697.57	5.45	736.03	**2.84**	517.36
	45°	43.01	5496.60	8.75	1038.17	42.97	4898.52	20.34	3903.85	8.46	1199.25	**3.98**	766.32
DTFPM	0°	0.87	—	0.87	—	1.21	—	1.00	—	**0.81**	—	0.94	—
	5°	1.02	17.23	1.16	32.78	1.55	27.63	1.43	43.49	**0.98**	21.74	1.32	40.58
	10°	1.40	60.34	1.35	54.67	1.97	62.64	1.79	79.82	**0.98**	20.75	1.45	53.82
	15°	1.96	124.60	1.52	73.39	2.85	135.10	1.85	85.83	**1.44**	78.66	1.52	61.62
	20°	2.65	203.56	2.00	128.99	3.86	218.31	2.32	132.46	**1.89**	133.40	1.97	109.50
	25°	4.16	375.71	**2.38**	172.86	5.14	323.97	3.68	269.44	2.87	255.74	3.12	231.59
	30°	6.05	591.73	**3.31**	278.31	7.43	512.76	5.79	480.59	4.35	438.76	5.16	448.71
	35°	9.12	943.91	**4.53**	417.93	10.62	775.74	8.10	711.94	6.78	739.54	7.14	658.74
	40°	13.50	1445.01	**6.37**	628.50	14.70	1111.82	9.78	881.15	9.74	1105.54	8.64	818.49
	45°	17.33	1883.09	**8.66**	891.01	18.35	1413.10	12.81	1184.81	13.83	1612.08	11.50	1122.53
WLD	0°	0.92	—	0.92	—	1.13	—	0.72	—	0.78	—	**0.65**	—
	5°	0.84	-8.61	1.02	9.90	1.28	12.95	0.75	4.51	0.79	2.26	**0.57**	-12.23
	10°	1.10	18.87	1.11	20.42	1.37	20.98	0.84	17.64	1.03	32.92	**0.70**	7.09
	15°	1.38	49.90	1.24	34.32	1.61	42.83	0.91	26.85	1.14	47.12	**0.87**	33.49
	20°	2.30	149.57	1.46	58.43	2.69	137.91	1.31	82.31	1.47	89.50	**1.14**	75.06
	25°	4.25	360.57	2.01	117.74	5.54	390.24	1.92	168.44	2.00	157.62	**1.49**	128.60
	30°	9.29	905.55	2.64	185.55	11.85	949.21	2.89	304.11	2.63	239.51	**1.99**	204.40
	35°	21.26	2202.19	3.88	319.93	23.47	1977.35	5.43	658.91	3.98	413.17	**2.60**	298.77
	40°	35.06	3696.61	6.22	573.82	35.86	3074.41	12.08	1587.46	6.03	677.38	**4.12**	531.52
	45°	43.34	4593.00	8.72	843.73	43.31	3734.29	24.35	3301.41	10.24	1219.98	**5.98**	815.63
GF	0°	1.02	—	1.02	—	2.15	—	0.40	—	0.76	—	**0.38**	—
	5°	1.50	47.55	1.29	27.41	2.81	30.95	0.60	51.87	1.02	33.54	**0.46**	20.50
	10°	2.34	130.05	1.52	50.01	4.01	86.47	0.67	67.88	1.32	72.96	**0.41**	7.95
	15°	3.90	283.84	1.94	90.97	5.20	142.12	0.97	144.29	1.87	145.91	**0.59**	53.55
	20°	7.16	604.34	2.93	188.74	8.88	313.38	1.77	343.63	2.91	281.76	**1.00**	161.08
	25°	13.57	1234.95	4.80	372.34	15.53	622.82	2.87	620.23	5.02	559.12	**1.63**	327.61
	30°	23.21	2183.73	7.95	681.83	25.30	1077.10	5.57	1300.74	8.32	992.67	**2.84**	643.92
	35°	37.14	3554.99	12.59	1138.61	37.79	1658.20	10.57	2556.57	14.09	1749.70	**4.79**	1156.47
	40°	46.26	4452.59	19.42	1810.58	46.45	2061.23	20.10	4951.93	21.49	2722.22	**8.22**	2053.95
	45°	48.05	4628.08	26.92	2549.20	48.05	2135.60	34.55	8585.07	28.78	3678.84	**12.74**	3238.87
SIFT	0°	1.80	—	1.80	—	2.02	—	1.32	—	1.54	—	**1.25**	—
	5°	2.30	28.26	2.05	14.14	2.46	22.14	1.42	7.83	1.72	11.83	**1.37**	9.34
	10°	2.56	42.53	2.19	21.80	2.75	36.10	1.80	36.72	2.43	57.96	**1.71**	36.39
	15°	4.11	129.08	2.78	54.57	4.27	111.53	2.40	82.42	3.08	99.82	**2.19**	75.02
	20°	5.51	206.72	3.68	105.09	6.66	229.92	3.46	162.95	3.48	125.56	**2.49**	99.44
	25°	8.65	381.87	4.36	142.66	9.02	347.11	4.25	222.54	5.41	251.16	**3.78**	202.50
	30°	12.69	606.56	5.72	218.46	12.99	543.57	6.16	367.81	8.74	467.17	**5.05**	303.86
	35°	16.32	808.88	8.11	351.76	17.11	747.91	8.70	560.13	11.59	652.31	**7.89**	531.20
	40°	22.96	1178.52	11.81	557.49	23.38	1058.67	11.52	774.49	17.10	1010.00	**10.15**	711.13
	45°	27.77	1446.86	**15.70**	774.65	27.83	1279.11	16.46	1149.28	22.84	1382.10	15.94	1174.38
ASAVE	0°	2.96	—	2.96	—	3.27	—	1.65	—	1.70	—	**1.34**	—
	5°	3.66	23.83	3.01	1.77	4.12	26.17	1.91	15.41	1.83	8.09	**1.46**	9.56
	10°	5.57	88.29	2.87	-3.02	6.03	84.71	2.70	63.39	2.24	31.89	**1.65**	23.41
	15°	8.12	174.78	2.98	0.70	8.56	162.14	4.29	159.54	2.47	45.53	**2.11**	58.06
	20°	10.54	256.54	3.40	15.04	11.34	247.16	6.44	289.15	3.22	89.84	**3.08**	130.70
	25°	11.87	301.71	**3.89**	31.63	13.06	299.75	8.19	395.30	5.29	211.86	4.70	251.85
	30°	14.57	392.87	**4.78**	61.84	16.28	398.43	10.01	505.31	9.51	460.02	7.16	435.72
	35°	20.66	598.91	**5.85**	97.88	22.78	597.45	11.40	589.44	15.33	803.39	10.53	687.56
	40°	30.83	943.09	**7.08**	139.41	31.61	867.82	14.61	783.26	19.70	1060.49	15.08	1028.66
	45°	38.58	1205.26	**11.51**	289.26	38.39	1075.56	22.94	1287.11	21.43	1162.75	19.60	1366.53

F. Rotation Compensation Using Geometric Shape Analysis

In this experiment, the performance of the method proposed in [2] is analysed as described in Section III-B. As neither an implementation nor the data set on which the shape analysis is based are available, the results on the original data cannot be reproduced. The main task of this approach is the detection of

TABLE IV
ACCURACY OF JOINT DETECTION USING A SLIDING WINDOW APPROACH AS PROPOSED IN [23]. THE PERCENTAGE IS THE DEVIATION OF THE DETECTED JOINT RELATIVE TO THE GROUND TRUTH WITH RESPECT TO THE LENGTH OF THE FINGER

	Deviation within			
	0-5%	5-10%	10-20%	>20%
Joint 1	74.80	6.36	9.78	9.06
Joint 2	51.67	27.42	13.20	7.71

TABLE V
STATISTICAL DATA OF THE FINGER GEOMETRY ON THE PLUSVEIN-FR DATA SET AS DEFINED IN TABLE 2 OF [2]

Gen	Fing	Value	Min	Mean	Max	Std Dev
M	Idx	$r_{root-tip}$	0.97	1.21	1.59	0.091
		r_{joints}	1.06	1.16	1.27	0.040
		$r_{joint1-tip}$	1.07	1.18	1.38	0.058
		$r_{root-joint1}$	0.86	1.02	1.16	0.055
		α	171.55	176.93	181.89	1.675
	Mid	$r_{root-tip}$	0.87	1.07	1.34	0.086
		r_{joints}	1.01	1.15	1.28	0.053
		$r_{joint1-tip}$	0.96	1.18	1.36	0.064
		$r_{root-joint1}$	0.74	0.91	1.15	0.072
		α	164.43	174.24	184.95	2.945
F	Idx	$r_{root-tip}$	0.94	1.25	1.63	0.126
		r_{joints}	1.05	1.19	1.32	0.056
		$r_{joint1-tip}$	1.02	1.20	1.43	0.073
		$r_{root-joint1}$	0.86	1.04	1.29	0.088
		α	170.41	176.62	181.68	2.405
	Mid	$r_{root-tip}$	0.87	1.07	1.36	0.096
		r_{joints}	1.05	1.18	1.32	0.054
		$r_{joint1-tip}$	0.99	1.19	1.40	0.062
		$r_{root-joint1}$	0.73	0.90	1.12	0.073
		α	168.81	173.92	182.11	2.329
All	All	$r_{root-tip}$	0.87	1.15	1.63	0.127
		r_{joints}	1.01	1.17	1.32	0.053
		$r_{joint1-tip}$	0.96	1.19	1.43	0.065
		$r_{root-joint1}$	0.73	0.97	1.29	0.095
		α	164.43	175.45	184.95	2.739

the finger lines and joints. For the joint detection, Chen *et al.* used a sliding window approach presented in [23]. As this algorithm did not provide satisfactory results for our data set, the joints as well as the roots and tips of the finger were marked manually. When comparing the manually determined values with those of the sliding window approach, large deviations are noticeable. Table IV states the results in detail. For joint 1 (proximal inter-phalangeal joint), 75% of the detected joints are within a range of 5% of the length of the finger (distance between finger root and -tip), for joint 2 (distal inter-phalangeal joint) only 52% are within this range. For joint 1 and joint 2, around 9% and nearly 8% of the detected joint positions are more than 20% off from the manually selected position, respectively.

The statistical measures obtained for the PLUSVein-FR are depicted in Table V. The values differ from the ones by Chen *et al.*, especially the angle α at the proximal inter-phalangeal joint is larger. The standard deviations differ as well: For the distance and diameter ratio values ($r_{root-tip}$, r_{joints}, $r_{joint1-tip}$ and $r_{root-joint1}$), the obtained one is 10 times higher, for α it is more than 10 times lower. These differences might result from the difference in the number of subjects and the subjects' ethnicity. Their data set consists of 12 Asian subjects (6 female and 6 male) only, whereas the PLUSVein-FR consists of 63 (27 female, 36 men) mainly European people.

Based on this statistical data, the geometric finger analysis to detect the finger rotation is executed for all rotation angles.

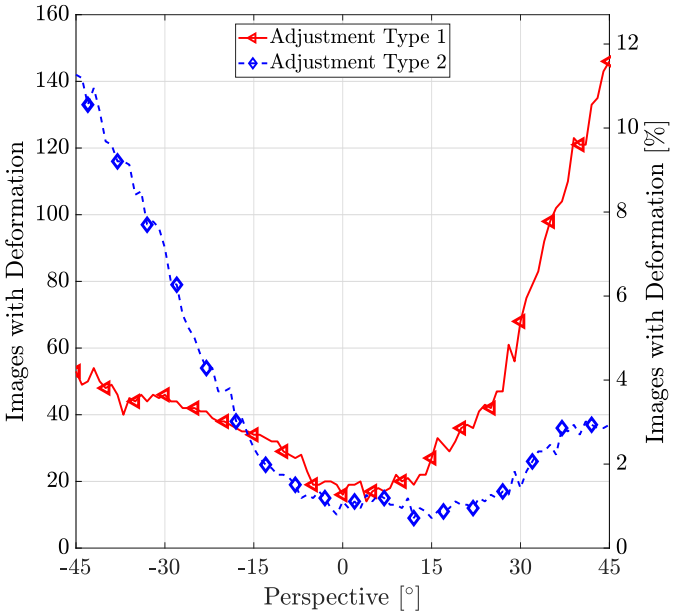

Fig. 12. Number of images with a detected longitudinal finger rotation (type 3 deformation) using the method presented in [2]. Left y-axis: absolute number of deformed images detected, right y-axis: value in percent (the total number of images is 1260).

Fig. 12 illustrates the number of detected images exhibiting longitudinal finger rotation. At a rotation angle of ±30°, less than 6% of the input images are detected as rotated, whereas for more than 2% a wrong (opposite direction) rotation is detected. Even at ±45° only 12% of the images are classified to contain a type 3 deformation. Thus, this method is clearly not applicable to the PLUSVein-FR. One reason therefore might be due to the placement of the finger. Chen *et al.* used a device where the finger is placed over its entire length on the scanner, while the PLUSVein-FR was captured with a device where only the fingertip and the finger trunk rests. The rest of the finger does not touch any part of the scanner. When placing a finger onto a surface, the finger is slightly deformed. This deformation influences the geometric properties on which Chen *et al.*'s algorithm is based. Due to the improper rotation detection, the recognition performance is not significantly improved compared to the unmodified data set. On the contrary, the performance even slightly decreases. This result seems to be valid as, e.g., for the SDUMLA-HMT Chen *et al.* only achieved an average RPI of 22% over all 7 investigated algorithms when applying corrections for all three analysed finger deformations. For MC, the RPI was 7% only (the EER decreased from 2.44% to 2.38%). These results indicate, that the performance gain will be even smaller if only a single correction is applied. The trend for GADC is basically the same as for the baseline results in Fig. 9, hence there is no separate visualization for GADC. However, the performance trend for GADC is depicted in the plots of Fig. 17, where all recognition schemes are compared.

G. Rotation Compensation Using Elliptic Pattern Normalization

In this part of the experiment, the EPN as proposed by Huang *et al.* [5] and described in Section III-C is applied.

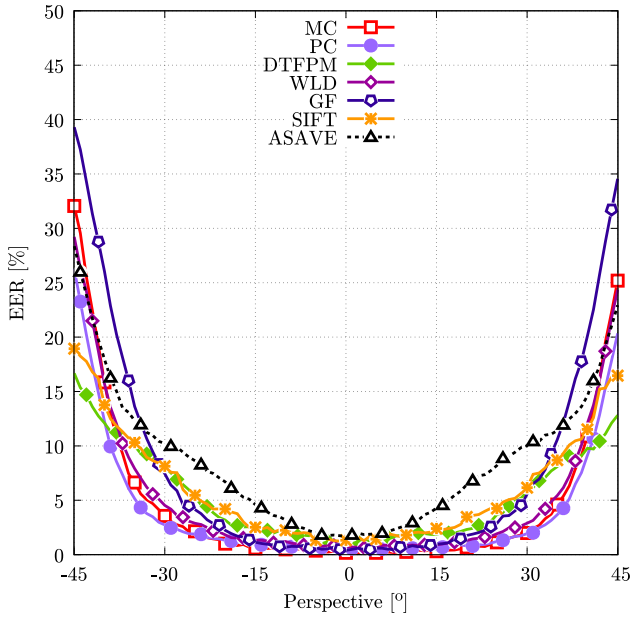

Fig. 13. Trend of the EER across the different rotation angles after applying EPN in the range of −45° to 45°.

Fig. 13 depicts the trend of the EER for elliptic input image normalization. The area in which the performance remains almost stable becomes larger for all recognition schemes. All algorithms, but especially MC, PC and WLD, show an increased robustness against longitudinal rotation. For MC, PC and WLD, the point at which the performance begins to degrade sharply, shifts to $> \pm 30°$ and to $> \pm 25°$ for GF. For DTFPM and SIFT, the performance curve flattens out compared to the unmodified data set. The same holds for ASAVE, which achieves the worst performance in terms of EER.

H. Rotation Compensation Using a Fixed Rotation Angle

The last part of the experiments is devoted to the analysis of the proposed rotation compensation method based on a fixed rotation angle as described in Section III-D. The top plot of Fig. 14 shows the functional principle using MC features for $\varphi_{corr} = 20$. It shows five different lines: one line for the trend of the EER of the unmodified data set, two lines for the $\pm\varphi_{corr}$ rotated images, the result of the maximum rule score level fusion from the original and the two fixed angle corrected scores and as a reference and a line for the performance using the known rotation angle for correction. Within the region of $\pm\varphi_{corr}$, the fused results are equal to the exact correction. Outside this region they stick to the angle corrected lines. That the performance of the proposed method is close to the performance of the known angle approach confirms the effectiveness of the approach. To show the influence of the pre-defined rotation angle φ_{corr} on the results, it is varied between 5°, 10°, 15°, 20° and 25° and applied on the PLUSVein-FR. The results are visualized in the bottom plot of Fig. 14: in essence, all curves follow the same trend, but the rotation angle at which the performance starts to decrease rapidly rises with an increasing φ_{corr}.

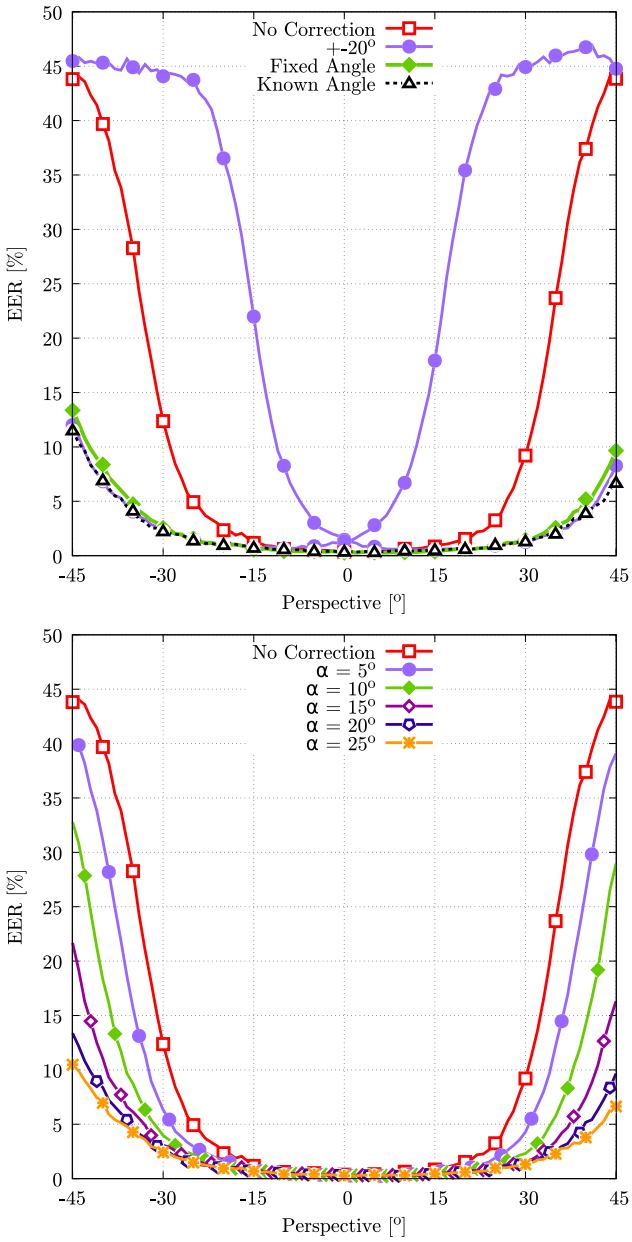

Fig. 14. Trend of the EER across the different perspectives applying a rotation compensation using a fixed rotation angle using MC features. Top: details for $\varphi = 20°$, bottom: the influence of varying φ from 5° to 25° in steps of 5°.

In the next experiment, the proposed fixed angle approach is applied on two different data sets with a correction angle of $\varphi_{corr} = 20°$: first to the original PLUSVein-FR and second to the PLUSVein-FR after elliptical pattern normalization has been performed. As all analysed recognition schemes are able to tolerate rotations to at least $\pm 10°$ a φ_{corr} of 20° is chosen, which keeps the effective rotation angle below 10° within a range of $\pm 30°$. Fig. 15 shows the results for both data sets. The top plot visualizes the EER values for the original data set. By applying the proposed approach, all evaluated recognition schemes achieve superior results compared to the original data set. The performance degradation is slower which, leading to flatter EER curves. Especially vein pattern based methods,

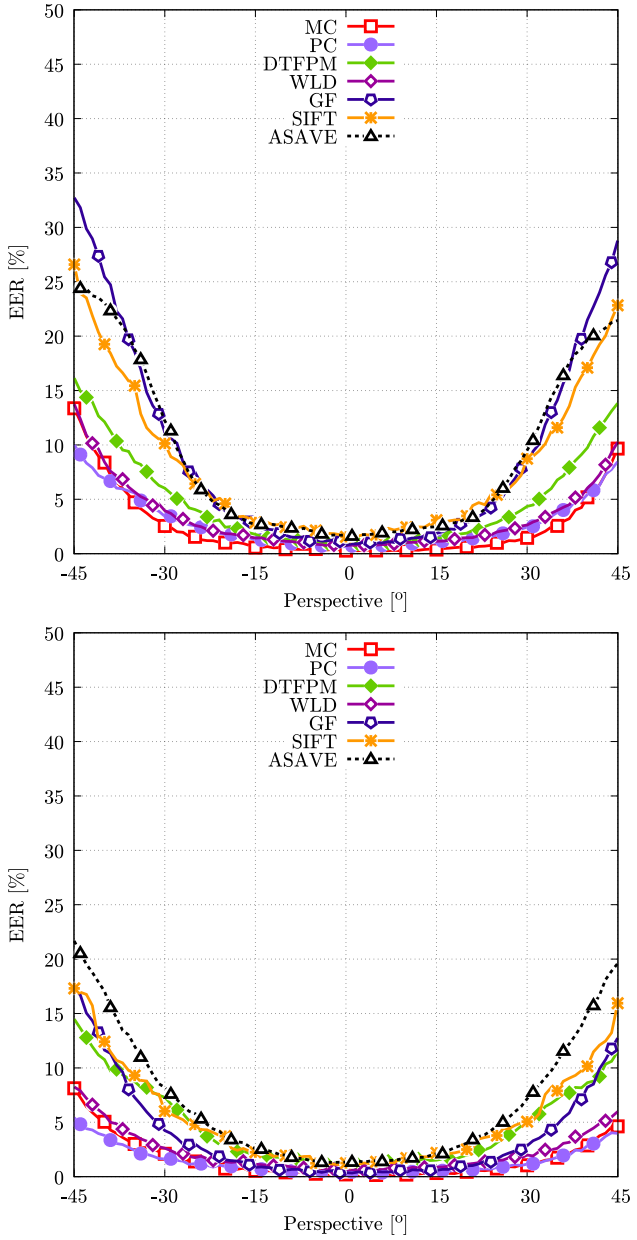

Fig. 15. Trend of the EER across the different perspectives applying a rotation compensation using a fixed rotation angle using MC features. Top: fixed angle compensation $\varphi = 20°$, bottom: fixed angle compensation combined with EPN.

namely MC, PC and WLD, benefit from this approach: there is no sharp drop in their performance any more: PC's EER stays below 10% over the whole range, MC's and WLD's below 14%. DTFPM achieves an EER just above 15% at ±45°, which is worse than the vein pattern based methods. SIFT and ASAVE arrive at EERs around 25%, GF at less than 35% for this rotation angle. The results for applying the proposed method together with EPN, which are depicted at the bottom of Fig. 15, are even superior. The curves are flatter compared to the original data set. The EER for PC stays below 5% over the whole range of ±45°, for MC and WLD below 10%, for DTFPM below 15% and for GF and SIFT below 20%. For the worst-performing algorithm, ASAVE, the EER only slightly exceeds 20%.

TABLE VI
EVALUATION RESULTS FOR THE METHOD PROPOSED IN SECTION III-D ON THE UTFVP DATA SET

Fixed Rotation Angle					
α	EER	FMR100	FMR1000	ZeroFMR	RPI
—	0.38 (±0.08)	0.23	0.50	2.19	—
±5°	0.14 (±0.05)	**0.09**	**0.14**	1.22	174.80
±10°	**0.14 (±0.05)**	0.10	0.17	**1.06**	**175.60**
±15°	0.16 (±0.05)	0.12	0.19	1.37	144.50
±20°	0.24 (±0.06)	0.14	0.42	2.50	57.35
±25°	0.30 (±0.07)	0.24	0.47	1.91	29.56
±30°	0.34 (±0.08)	0.26	0.49	2.08	11.49
±35°	0.50 (±0.09)	0.40	0.89	2.48	-24.14
±40°	1.89 (±0.18)	2.73	6.35	21.13	-79.81
±45°	7.39 (±0.34)	14.72	22.88	34.31	-94.83
Fixed Rotation Angle + EPN					
α	EER	FMR100	FMR1000	ZeroFMR	RPI
—	0.35 (±0.08)	0.24	0.56	2.16	—
±5°	**0.17 (±0.05)**	0.14	**0.19**	**0.66**	**100.80**
±10°	0.21 (±0.06)	0.16	0.24	1.01	67.39
±15°	0.17 (±0.05)	**0.12**	0.26	1.32	100.80
±20°	0.19 (±0.06)	0.16	0.30	1.35	81.84
±25°	0.21 (±0.06)	0.17	0.24	1.60	66.77
±30°	0.28 (±0.07)	0.19	0.35	1.55	24.90
±35°	0.31 (±0.07)	0.23	0.54	1.81	10.83
±40°	0.61 (±0.10)	0.45	1.61	14.20	-42.79
±45°	0.87 (±0.12)	0.80	1.75	7.60	-59.98

I. *Verification of the Fixed Rotation Angle Approach*

To verify the effectiveness of the proposed fixed angle approach, it is applied on the publicly available UTFVP [10] and SDUMLA-HMT [11] data sets. Both data sets consist of finger vein images acquired from the palmar perspective. Again, we use the original data set and its elliptic normalized version during the experiments. φ_{corr} is varied from 5° to 45° in steps of 5°. This part of the experiment is only performed for MC features.

By visual inspection, the UTFVP data set seems to exhibit little to no longitudinal rotation, whereas the extent of longitudinal finger rotation within SDUMLA-HMT seems to be higher. Table VI lists the results for the UTFVP data set. The baseline EER without any rotation correction is 0.38%. Using the fixed angle correction approach, the EER reaches its minimum of 0.14% for $\varphi_{corr} = 10°$ and keeps below 0.34% until $\varphi_{corr} \leq 30°$. With a further increase of φ_{corr}, the performance drops faster and hits an EER of 7.39%. FMR100, FMR1000 and ZeroFMR follow approximately the same trend. The last column shows the *RPI* with respect to the baseline EER. At its maximum, the relative performance increase is 175%. By applying EPN on the data set the EER without fixed angle correction arrives at 0.35%, corresponding to an RPI of 20% compared to the baseline performance on the unchanged data set. When combining both methods, the best result with an EER of 0.17% is achieved for $\varphi_{corr} = 5°$. This corresponds to an RPI of 100% and 145% compared to the elliptic normalized data set without fixed angle correction and to the original unmodified data set, respectively.

The results for the SDUMLA-HMT data set are listed in Table VII. The baseline EER is 4.19% for the unmodified data set. By applying the proposed approach with increasing φ_{corr}, the EER steadily drops until $\varphi_{corr} = 25°$ where it reaches its minimum of 1.62%. If φ is further increased, the EER increases rapidly to an EER around 9.5%. Again, FMR100,

TABLE VII
EVALUATION RESULTS FOR THE METHOD PROPOSED IN SECTION III-D ON THE SDUMLA-HMT DATA SET

Fixed Rotation Angle					
α	EER	FMR100	FMR1000	ZeroFMR	RPI
—	4.19 (±0.13)	5.29	7.01	52.78	—
±5°	3.13 (±0.12)	3.93	5.62	63.36	33.71
±10°	2.41 (±0.10)	2.85	4.30	55.24	73.95
±15°	2.01 (±0.09)	2.41	3.50	**51.88**	108.10
±20°	1.72 (±0.09)	1.97	3.14	52.10	143.80
±25°	**1.62 (±0.09)**	**1.84**	**3.11**	60.29	**157.90**
±30°	1.71 (±0.09)	2.02	3.36	56.76	144.40
±35°	2.00 (±0.09)	2.45	4.55	73.00	109.00
±40°	3.96 (±0.13)	6.55	13.49	80.94	5.71
±45°	9.54 (±0.20)	17.94	27.67	85.68	-56.10
Fixed Rotation Angle + EPN					
α	EER	FMR100	FMR1000	ZeroFMR	RPI
—	2.18 (±0.10)	2.55	3.63	46.43	—
±5°	1.61 (±0.08)	1.80	2.94	53.17	35.94
±10°	1.49 (±0.08)	1.59	2.38	42.30	46.86
±15°	1.29 (±0.08)	1.36	2.13	**40.57**	69.41
±20°	1.11 (±0.07)	1.13	**1.90**	42.40	96.60
±25°	**1.05 (±0.07)**	**1.06**	1.94	49.46	**108.80**
±30°	1.25 (±0.07)	1.36	2.35	47.94	74.25
±35°	1.52 (±0.08)	1.74	2.94	52.21	43.67
±40°	1.82 (±0.09)	2.17	4.05	64.33	20.23
±45°	2.18 (±0.10)	2.93	5.77	61.49	0.12

FMR1000 and ZeroFMR show approximately the same trend. The maximum *RPI* is 158% for $\varphi_{corr} = 25°$. By applying EPN on the data set, the EER arrives at 2.18%, which corresponds to an RPI of 92% compared to the baseline performance. Combining both methods further improves the results, hitting the best performance at $\varphi_{corr} = 25°$ with an EER of 1.05%. The resulting RPI is 109% and 300% with respect to the elliptic normalized data set and to the original unmodified data set, respectively.

As the rotation angle of 25°, where the best result is achieved, seems to be relatively high, we checked the result for plausibility by visually inspecting the images manually. It turned out that there are quite a view samples exhibiting a high degree of longitudinal rotation. Fig. 16 shows such an example (sample number 2 and 3 of the left ring finger from subject #6). The top row shows the original images from the data set. It is clearly visible that the two finger images are rotated versions of each other. The second and third row show the ROI of the left and right sample, respectively. The bottom row is the rotation corrected right image using a rotation angle of 25°. The vein pattern of the rotated version of the right image is clearly more similar to sample #2 than the original features of sample #3.

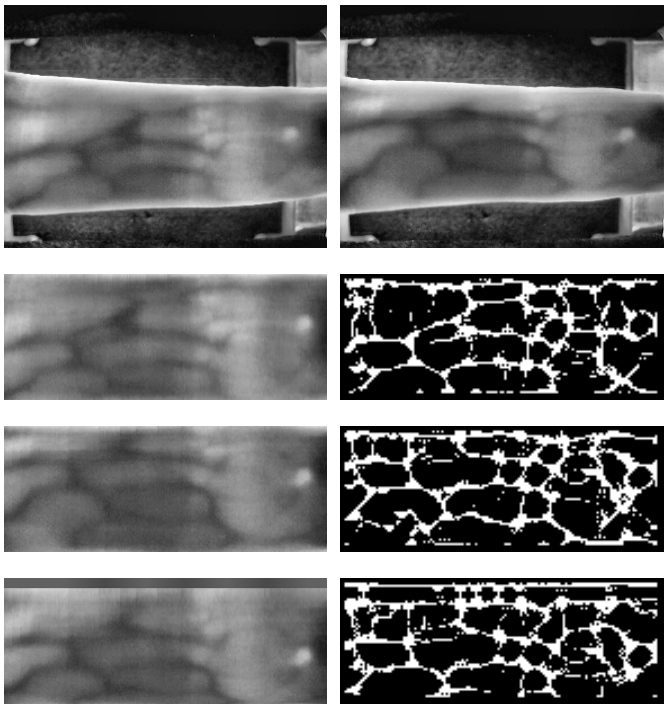

Fig. 16. Example of two samples from the same finger of the SDUMLA-HMT data set. Top row: original images, row 2: ROI and extracted features from the left sample, row 3: right sample, bottom row: rotated version of the right sample using a rotation angle of 25°.

J. Comparison of Rotation Compensation Methods

To enable a better comparison of the different rotation correction approaches' performance gain for each recognition scheme, Fig. 17 depicts their trends grouped per scheme. As all simple vein pattern based methods (MC, PC, WLD, GF) follow the same general behaviour, only MC is visualized. Table VIII lists the EER and the RPI with respect to the baseline performance of the unmodified data set at the palmar view for all correction / recognition scheme combinations for some selected perspectives.

The top-left figure gives the performance for MC. Like all vein pattern based methods, MC highly benefits from the rotation compensation. Without rotation correction, MC is able to achieve a relatively stable recognition rates up to a rotation angle of ±15°. For higher rotation angles, the performance drops faster, and starts to drop rapidly at ±25°. At ±45°, the EER is close to 45%. The recognition rate can be improved noticeably by applying a correction based on the actual known rotation angle. Hereby, the range, in which the performance is stable can be increased to ±30°. Even at ±45° the EER is still around 10%, which corresponds to an RPI of 600%. An application of GADC type 3 correction has no positive effect at all. On the contrary, the performance even slightly degrades. Similar to applying a correction using the known rotation angle, also EPN extends the stable region. However, starting at a rotation angle of ±30°, the recognition rate starts to decrease rapidly. Applying the proposed fixed angle method with a pre-defined rotation correction angle of $\varphi_{corr} = 20°$ achieves similar results to the known angle method. The best results are accomplished by combining the fixed angle method with EPN. This combination even outperforms the known angle correction method. The worst EER at $-45°$ is still 8%.

The DTFPM results are visualized in the top-right subplot. DTFPM is designed to be robust against longitudinal finger rotation. As a result, all curves are shallowed compared to MC. Even using the original, non-corrected data set yields EERs of $< 20\%$ over the whole tested range. Applying a correction using the known rotation angle doubles the performance, resulting in a maximum EER of about 10% at ±45°. Again, the application of GADC yields a slight deterioration of the performance. Elliptic normalization, the fixed angle method

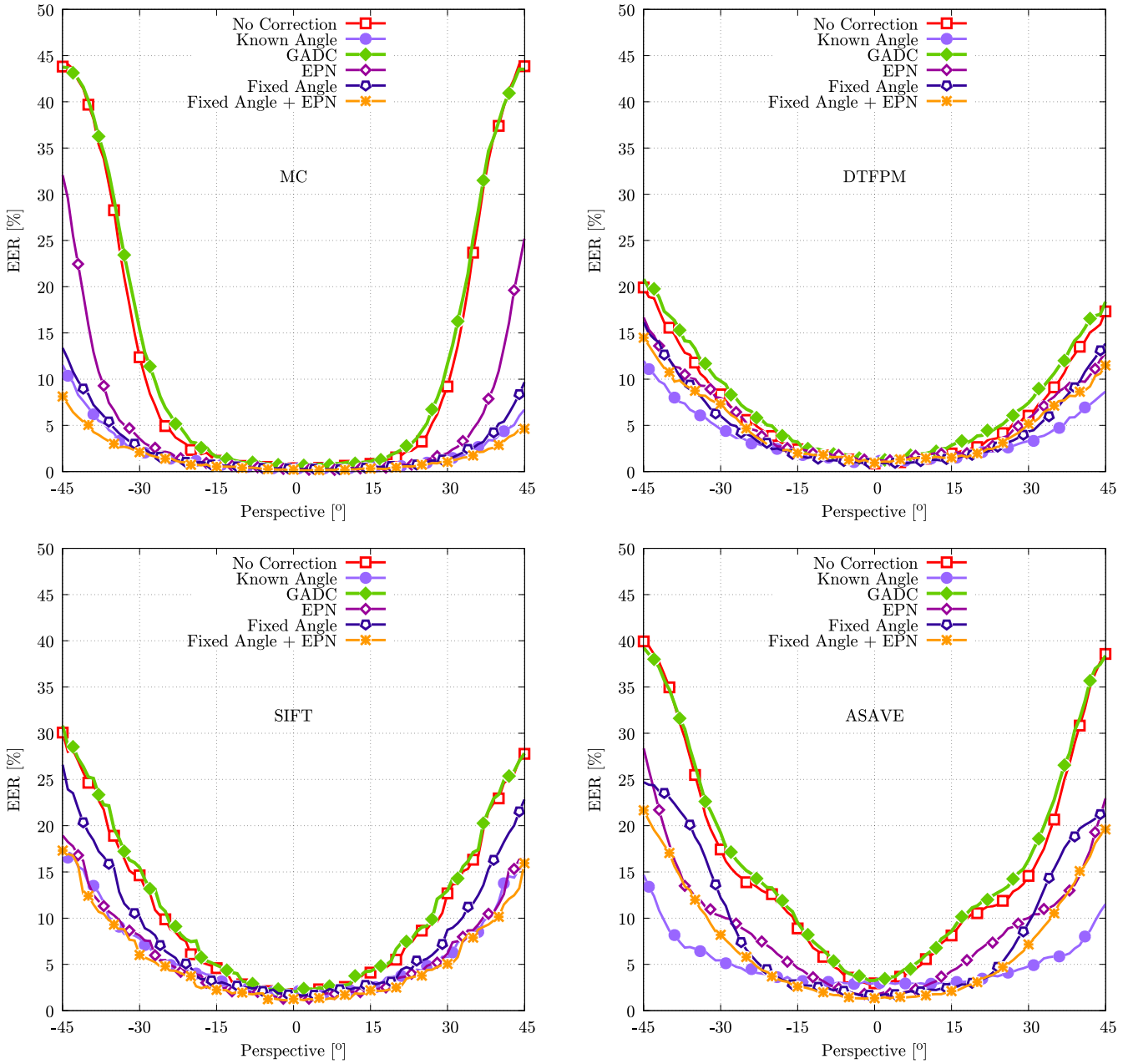

Fig. 17. Trend of the EER across the different perspectives applying different rotation compensation approaches for the same recognition scheme. Top left: MC, top right: DTFPM, bottom left: SIFT, bottom right: ASAVE.

and the combination of both are superior to no correction but inferior to the known angle method. The proposed fixed angle method achieves the best results among these methods for DTFPM.

Similar to DTFPM, SIFT is more robust against longitudinal finger rotation than vein pattern based methods. This leads to a similar behaviour for the different correction methods, although with raised EER rates: A correction using the known rotation angle flattens the EER curve, achieving an EER of just above 15% at ±45° (instead of 30% without correction). GADC does not improve the results at all. The proposed method also reduces the resulting EERs, but not to the same extent as the known angle method. EPN achieves roughly the same recognition rates as the correction using the known angle. The combination of elliptic normalization and the fixed angle method achieves the overall best results. The results are depicted in the bottom-left plot.

The bottom-right chart shows the results for ASAVE. The known angle correction achieves pretty stable results within the range of ±40° with an EER below 8%. For higher rotation angles the performance drops sharply until it reaches its maximum EER of 15% at −45°. Again, GADC does not gain any performance increase compared to the performance of the original data set. Elliptic normalization shallows the EER curve and achieves EERs below 10% up to ±30°. For higher rotation angles its performance decreases rapidly and arrives at an EER of 23% at ±45°. The proposed method is

TABLE VIII
PERFORMANCE RESULTS IN TERMS OF EER AND RPD OF ALL CORRECTION METHODS AND RECOGNITION SCHEMES. THE RPI IS ALWAYS CALCULATED WITH RESPECT TO THE BASELINE PERFORMANCE OF THE UNMODIFIED DATA SET AT THE PALMAR VIEW FOR ALL CORRECTION / RECOGNITION SCHEME COMBINATIONS. THE HIGHLIGHTED RESULTS (BOLD FACE) REPRESENT THE BEST RECOGNITION RATES FOR A RECOGNITION SCHEME AT THE SPECIFIED ROTATION ANGLE

Method	Rotation angle	No Correction		Known Angle		GADC		EPN		Fixed Angle		Fixed Angle + EPN	
		EER	RPI	EER	RPI	EER	RPI	EER	RPI	EER	RPI	EER	RPI
MC	0°	0.37	—	0.37	—	0.59	-38.28	**0.17**	112.05	0.28	28.75	0.21	77.65
	5°	0.41	—	0.34	23.33	0.81	-49.13	0.17	137.62	0.30	37.19	**0.16**	161.92
	10°	0.63	—	0.49	28.90	0.96	-34.07	0.25	149.68	0.32	98.65	**0.19**	233.88
	15°	0.84	—	0.52	61.47	1.11	-23.84	**0.32**	165.33	0.38	122.12	0.34	151.72
	20°	1.54	—	0.62	149.10	2.05	-25.06	0.67	130.62	0.62	148.55	**0.44**	246.90
	25°	3.25	—	0.99	229.82	4.42	-26.51	1.13	187.42	1.00	224.69	**0.75**	335.93
	30°	9.21	—	1.32	598.55	11.66	-21.04	1.99	363.26	1.46	530.78	**1.05**	780.21
	35°	23.68	—	2.03	1069.22	25.21	-6.07	4.61	413.90	2.55	827.58	**1.74**	1258.25
	40°	37.39	—	3.93	851.27	37.85	-1.21	10.88	243.70	5.19	621.04	**2.88**	1199.62
	45°	43.84	—	6.69	555.26	43.51	0.77	25.19	74.03	9.66	353.88	**4.62**	848.20
PC	0°	0.77	—	0.77	—	0.86	-10.59	0.51	51.26	0.65	17.98	**0.46**	67.14
	5°	0.75	—	0.76	-2.09	0.78	-4.13	0.51	47.17	0.65	14.83	**0.43**	74.82
	10°	0.89	—	0.87	1.83	0.98	-9.46	0.49	81.44	0.92	-3.22	**0.41**	116.07
	15°	1.13	—	1.11	1.43	1.26	-10.19	0.52	115.55	0.97	16.81	**0.46**	145.78
	20°	1.65	—	1.48	11.66	1.81	-8.93	0.81	103.94	1.34	23.58	**0.63**	161.22
	25°	3.26	—	1.62	101.18	3.84	-15.00	1.21	170.37	1.70	91.82	**0.86**	279.37
	30°	6.52	—	2.56	154.87	8.37	-22.06	1.94	236.61	2.44	167.50	**1.16**	462.62
	35°	15.36	—	3.93	290.30	17.91	-14.27	3.67	317.96	3.79	305.27	**1.78**	763.27
	40°	30.37	—	6.06	400.87	31.64	-4.03	9.13	232.48	5.45	457.58	**2.84**	969.69
	45°	43.01	—	8.75	391.72	42.97	0.11	20.34	111.44	8.46	408.21	**3.98**	979.76
DTFPM	0°	0.87	—	0.87	—	1.21	-27.93	1.00	-12.34	**0.81**	8.18	0.94	-7.07
	5°	1.02	—	1.16	-11.71	1.55	-33.81	1.43	-28.38	**0.98**	4.17	1.32	-22.50
	10°	1.40	—	1.35	3.66	1.97	-28.95	1.79	-21.83	**0.98**	43.66	1.45	-3.12
	15°	1.96	—	1.52	29.53	2.85	-31.15	1.85	5.95	**1.44**	36.00	1.52	29.15
	20°	2.65	—	2.00	32.56	3.86	-31.27	2.32	14.47	**1.89**	40.70	1.97	34.66
	25°	4.16	—	**2.38**	74.35	5.14	-19.14	3.68	12.88	2.87	44.67	3.12	33.33
	30°	6.05	—	**3.31**	82.85	7.43	-18.65	5.79	4.44	4.35	38.90	5.16	17.16
	35°	9.12	—	**4.53**	101.55	10.62	-14.09	8.10	12.71	6.78	34.52	7.14	27.86
	40°	13.50	—	**6.37**	112.08	14.70	-8.12	9.78	38.04	9.74	38.64	8.64	56.33
	45°	17.33	—	**8.66**	100.11	18.35	-5.55	12.81	35.31	13.83	25.31	11.50	50.75
WLD	0°	0.92	—	0.92	—	1.13	-18.25	0.72	29.02	0.78	19.02	**0.65**	41.42
	5°	0.84	—	1.02	-16.85	1.28	-33.86	0.75	12.82	0.79	6.36	**0.57**	47.24
	10°	1.10	—	1.11	-1.29	1.37	-19.67	0.84	30.36	1.03	6.43	**0.70**	56.97
	15°	1.38	—	1.24	11.60	1.61	-14.20	0.91	52.46	1.14	21.26	**0.87**	58.80
	20°	2.30	—	1.46	57.53	2.69	-14.24	1.31	76.62	1.47	56.74	**1.14**	101.62
	25°	4.25	—	2.01	111.52	5.54	-23.19	1.92	121.36	2.00	112.78	**1.49**	184.92
	30°	9.29	—	2.64	252.15	11.85	-21.65	2.89	221.04	2.63	252.50	**1.99**	367.17
	35°	21.26	—	3.88	448.23	23.47	-9.40	5.43	291.39	3.98	433.94	**2.60**	716.45
	40°	35.06	—	6.22	463.45	35.86	-2.22	12.08	190.28	6.03	481.27	**4.12**	750.19
	45°	43.34	—	8.72	397.28	43.31	0.06	24.35	78.01	10.24	323.15	**5.98**	624.84
GF	0°	1.02	—	1.02	—	2.15	-52.71	0.40	155.42	0.76	33.43	**0.38**	166.30
	5°	1.50	—	1.29	15.80	2.81	-46.72	0.60	148.15	1.02	47.42	**0.46**	226.07
	10°	2.34	—	1.52	53.36	4.01	-41.66	0.67	250.00	1.32	77.48	**0.41**	467.51
	15°	3.90	—	1.94	100.99	5.20	-25.04	0.97	301.31	1.87	108.26	**0.59**	565.66
	20°	7.16	—	2.93	143.93	8.88	-19.43	1.77	305.52	2.91	146.17	**1.00**	618.42
	25°	13.57	—	4.80	182.63	15.53	-12.67	2.87	373.42	5.02	170.24	**1.63**	731.35
	30°	23.21	—	7.95	192.10	25.30	-8.26	5.57	316.43	8.32	178.87	**2.84**	717.49
	35°	37.14	—	12.59	195.09	37.79	-1.70	10.57	251.41	14.09	163.65	**4.79**	674.64
	40°	46.26	—	19.42	138.28	46.45	-0.39	20.10	130.17	21.49	115.24	**8.22**	462.84
	45°	48.05	—	26.92	78.47	48.05	0.00	34.55	39.05	28.78	66.95	**12.74**	277.09
SIFT	0°	1.80	—	1.80	—	2.02	-11.01	1.32	36.31	1.54	16.53	**1.25**	43.56
	5°	2.30	—	2.05	12.36	2.46	-6.56	1.42	62.14	1.72	33.65	**1.37**	68.40
	10°	2.56	—	2.19	17.02	2.75	-6.81	1.80	42.11	2.43	5.15	**1.71**	50.03
	15°	4.11	—	2.78	48.20	4.27	-3.63	2.40	71.17	3.08	33.59	**2.19**	87.90
	20°	5.51	—	3.68	49.55	6.66	-17.27	3.46	58.99	3.48	58.46	**2.49**	120.77
	25°	8.65	—	4.36	98.58	9.02	-4.09	4.25	103.64	5.41	59.91	**3.78**	128.68
	30°	12.69	—	5.72	121.87	12.99	-2.31	6.16	105.87	8.74	45.17	**5.05**	151.15
	35°	16.32	—	8.11	101.19	17.11	-4.61	8.70	87.67	11.59	40.79	**7.89**	106.71
	40°	22.96	—	11.81	94.45	23.38	-1.81	11.52	99.28	17.10	34.22	**10.15**	126.27
	45°	27.77	—	**15.70**	76.85	27.83	-0.19	16.46	68.78	22.84	21.62	15.94	74.25
ASAVE	0°	2.96	—	2.96	—	3.27	-9.49	1.65	78.74	1.70	74.16	**1.34**	121.18
	5°	3.66	—	3.01	21.68	4.12	-11.16	1.91	91.79	1.83	99.52	**1.46**	150.00
	10°	5.57	—	2.87	94.15	6.03	-7.74	2.70	105.97	2.24	148.63	**1.65**	237.44
	15°	8.12	—	2.98	172.88	8.56	-5.13	4.29	89.24	2.47	228.84	**2.11**	284.51
	20°	10.54	—	3.40	209.91	11.34	-7.05	6.44	63.76	3.22	227.09	**3.08**	241.82
	25°	11.87	—	**3.89**	205.17	13.06	-9.05	8.19	44.97	5.29	124.34	4.70	152.53
	30°	14.57	—	**4.78**	204.54	16.28	-10.50	10.01	45.54	9.51	53.28	7.16	103.49
	35°	20.66	—	**5.85**	253.19	22.78	-9.30	11.40	81.20	15.33	34.74	10.53	96.29
	40°	30.83	—	**7.08**	335.70	31.61	-2.45	14.61	111.09	19.70	56.54	15.08	104.41
	45°	38.58	—	**11.51**	235.32	38.39	0.49	22.94	68.20	21.43	80.02	19.60	96.86

able to keep the recognition rates stable between ±20°. For higher rotation angles the performance degrades sharply. Once more, the best results are achieved by using a combination of EPN and the proposed method. Although, for ASAVE the performance results in this case are noticeable worse compared to the correction using the known angle.

TABLE IX
RANKING OF THE ROTATION CORRECTION METHODS UNDER INVESTIGATION BASED ON THE EXPERIMENTAL RESULTS PER RECOGNITION SCHEME

Rotation correction	No Corr	Known Angle	GADC	EPN	Fixed Angle	Fixed Angle + EPN
MC	5	2	6	4	3	1
PC	5	2	6	4	3	1
DTFPM	5	1	6	4	2	3
WLD	5	2	6	4	3	1
GF	5	2	6	4	3	1
SIFT	5	2	6	3	4	1
ASAVE	5	1	6	4	3	2

K. Ranking of Rotation Correction Methods

Table IX gives the ranking of the applied rotation correction methods per recognition scheme. Regarding the single approaches, the correction using the known rotation angle achieves the best results. Although, in practical applications the known angle method cannot be applied as the rotation angle is usually not known. Thus, the most appropriate approach is the proposed fixed angle method on its own. However, a combination of the proposed approach and the EPN further improves the results. Especially for vein pattern based schemes, the results achieved by the proposed method are only slightly worse than the known angle approach. Except for SIFT, EPN on its own leads to inferior results compared to the proposed method. GADC even degrades the recognition rates compared to applying no correction.

The results of the different rotation correction approaches indicate that simple vein pattern based methods get the most out of rotation correction. MC, PC as well as WLD outperform all other recognition schemes after applying a rotation compensation using the exact rotation angle, elliptic normalization, the fixed angle method or a combination of the latter two.

L. Runtime Evaluation for Fixed Angle Approach

The rotation correction introduces additional processing steps. Thus, the runtime costs are relevant in a practical application. As the rotation compensation is applied during biometric enrolment, the additional cost are two comparisons and the maximum rule score level fusion at the biometric recognition. If the approach is combined with EPN, this step needs to be considered too. Note, that the implementations of the recognition algorithms used in these experiments are not optimized for runtime performance. Hence, the determined durations are only indicators for the additional costs imposed due to the proposed approach. Table X lists the average processing times for the different steps in the recognition tool-chain. It can be seen that the additional runtime of the steps added by this approach (two comparisons and the maximum score level fusion) is negligible compared to the other steps. Therefore, the total duration, as shown in Table XI, is only slightly higher. As the processing of the elliptical correction takes noticeably longer, its application increases the overall duration perceptibly. The runtime analysis shows, that the fixed angle correction approach on its own is suitable for real-time applications.

TABLE X
THE AVERAGE TIME OF COST FOR EVERY RELEVANT STEP IN THE RECOGNITION TOOL-CHAIN

Method	EPN [ms]	PP [ms]	FE [ms]	Comparison [ms]	Fusion [ms]
MC	89.942	29.705	293.114	2.621	0.006
PC	89.942	28.185	4.367	2.452	0.006
DTFPM	89.942	4.842	341.537	3.278	0.006
WLD	89.942	16.179	24.221	2.483	0.006
GF	89.942	84.456	6.107	2.472	0.006
SIFT	89.942	83.569	23.076	2.761	0.006
ASAVE	89.942	17.887	113.711	2.560	0.006

TABLE XI
THE AVERAGE TIME OF COST FOR A SINGLE COMPARISON USING NO ROTATION CORRECTION, THE FIXED ANGLE APPROACH AND THE FIXED ANGLE APPROACH AFTER APPLYING EPN

Method	No Correction	Fixed Angle		Fixed Angle + EPN	
	[s]	[s]	Increase [%]	[s]	Increase [%]
MC	0.325	0.331	1.61	0.421	29.25
PC	0.035	0.040	14.03	0.130	270.98
DTFPM	0.350	0.356	1.88	0.446	27.60
WLD	0.043	0.048	11.60	0.138	221.34
GF	0.093	0.098	5.32	0.188	102.00
SIFT	0.109	0.115	5.05	0.205	87.26
ASAVE	0.134	0.139	3.82	0.229	70.86

V. CONCLUSION

We systematically investigated the extent to which longitudinal finger rotation can be compensated and the impact of the correction on the recognition accuracy of a finger vein recognition system. Therefore, we evaluated two novel correction approaches and two other ones from the literature. The first approach has not been applied to finger vein recognition before and exploits the fact that for the PLUSVein-FR data set the angle of the longitudinal rotation is known. It applies a rotation compensation using a circular projection based on this known angle. As second approach we evaluated a method proposed by Chen *et al.* [2] that analyses the geometric shape of the finger and based on this results, detects deformations and corrects them. The third approach applies an elliptic pattern normalization as proposed in [5].

In real world scenarios the longitudinal rotation angle is unknown and its estimation is a difficult task. The fourth approach, is a novel method that is able to correct longitudinal finger rotation deformation without any knowledge or estimation of the actual angle of rotation, which is its main advantage.

The results of the known angle approach showed that a correction of the rotation is possible up to $\pm 30°$, achieving reasonable recognition results. It turned out that especially vein pattern based algorithms, e.g., MC and PC, benefit from this rotation correction. The approach based on the geometric shape analysis, did not achieve satisfactory results on our data set at all. By applying EPN, all recognition schemes under investigation achieved superior results compared to applying no correction. By successfully applying the newly proposed fixed angle method on three different data sets (PLUSVein-FR, UTFVP and SDUMLA-HMT), we confirmed its effectiveness. The analysis of the computational cost showed, that the fixed angle correction approach is also suitable for real-time applications. A combination with EPN further improved the results

and achieved the best robustness against longitudinal finger rotation for all recognition schemes. However, EPN is more computational expensive than the proposed approach.

We further confirmed that simple, vein pattern based recognition schemes in combination with our proposed correction method outperform more sophisticated and complex recognition algorithms and rotation detection frameworks. For example, PC with elliptic normalization and our proposed fixed angle compensation approach reduces the impact of longitudinal finger rotation noticeably. In biometrics there is a general trend towards contact-less as well as on-the-move acquisition. Hence, recognition tool-chains that are robust against different finger misplacements and the resulting deformations will become essential.

Our future work will include further analysis of deformations caused by different finger misplacements and the development of methodologies improving the robustness against them. Furthermore, we will analyse the presence of finger rotation in commonly used publicly available finger vein data sets.

REFERENCES

[1] A. Kumar and Y. Zhou, "Human identification using finger images," *IEEE Trans. Image Process.*, vol. 21, no. 4, pp. 2228–2244, Apr. 2012.

[2] Q. Chen, L. Yang, G. Yang, and Y. Yin, "Geometric shape analysis based finger vein deformation detection and correction," *Neurocomputing*, vol. 311, pp. 112–125, Oct. 2018.

[3] B. Prommegger, C. Kauba, and A. Uhl, "Longitudinal finger rotation—Problems and effects in finger-vein recognition," in *Proc. Int. Conf. Biometrics Special Interest Group (BIOSIG)*, Darmstadt, Germany, 2018, pp. 1–11.

[4] E. C. Lee, H. C. Lee, and K. R. Park, "Finger vein recognition using minutia-based alignment and local binary pattern-based feature extraction," *Int. J. Imag. Syst. Technol.*, vol. 19, no. 3, pp. 179–186, 2009.

[5] B. Huang, Y. Dai, R. Li, D. Tang, and W. Li, "Finger-vein authentication based on wide line detector and pattern normalization," in *Proc. IEEE 20th Int. Conf. Pattern Recognit. (ICPR)*, 2010, pp. 1269–1272.

[6] Y. Matsuda, N. Miura, A. Nagasaka, H. Kiyomiu, and T. Miyatake, "Finger-vein authentication based on deformation-tolerant feature-point matching," *Mach. Vis. Appl.*, vol. 27, no. 2, pp. 237–250, 2016.

[7] L. Yang, G. Yang, Y. Yin, and X. Xi, "Finger vein recognition with anatomy structure analysis," *IEEE Trans. Circuits Syst. Video Technol.*, vol. 28, no. 8, pp. 1892–1905, Aug. 2018.

[8] C. Kauba, B. Prommegger, and A. Uhl, "The two sides of the finger—Dorsal or palmar—Which one is better in finger-vein recognition?" in *Proc. Int. Conf. Biometrics Special Interest Group (BIOSIG)*, Darmstadt, Germany, 2018, pp. 1–5.

[9] B. Prommegger, C. Kauba, and A. Uhl, "Multi-perspective finger-vein biometrics," in *Proc. IEEE 9th Int. Conf. Biometrics Theory Appl. Syst. (BTAS)*, Los Angeles, CA, USA, 2018, pp. 1–9.

[10] B. T. Ton and R. N. J. Veldhuis, "A high quality finger vascular pattern dataset collected using a custom designed capturing device," in *Proc. Int. Conf. Biometrics (ICB)*, 2013, pp. 1–5. [Online]. Available: http://doc.utwente.nl/87790/

[11] Y. Yin, L. Liu, and X. Sun, "SDUMLA-HMT: A multimodal biometric database," in *Biometric Recognition*. Heidelberg, Germany: Springer, 2011, pp. 260–268.

[12] J. Zhao, H. Tian, W. Xu, and X. Li, "A new approach to hand vein image enhancement," in *Proc. 2nd Int. Conf. Intell. Comput. Technol. Autom. (ICICTA)*, vol. 1, 2009, pp. 499–501.

[13] J. Zhang and J. Yang, "Finger-vein image enhancement based on combination of gray-level grouping and circular Gabor filter," in *Proc. IEEE Int. Conf. Inf. Eng. Comput. Sci. (ICIECS)*, 2009, pp. 1–4.

[14] K. Zuiderveld, "Contrast limited adaptive histogram equalization," in *Graphics Gems IV*, P. S. Heckbert, Ed. San Diego, CA, USA: Morgan Kaufmann, 1994, pp. 474–485.

[15] C. Kauba, J. Reissig, and A. Uhl, "Pre-processing cascades and fusion in finger vein recognition," in *Proc. Int. Conf. Biometrics Special Interest Group (BIOSIG)*, Darmstadt, Germany, Sep. 2014, pp. 1–6.

[16] N. Miura, A. Nagasaka, and T. Miyatake, "Extraction of finger-vein patterns using maximum curvature points in image profiles," *IEICE Trans. Inf. Syst.*, vol. 90, no. 8, pp. 1185–1194, 2007.

[17] J. H. Choi, W. Song, T. Kim, S.-R. Lee, and H. C. Kim, "Finger vein extraction using gradient normalization and principal curvature," in *Proc. SPIE Image Process. Mach. Vis. Appl.*, vol. 7251, 2009, Art. no. 725111. [Online]. Available: https://doi.org/10.1117/12.810458

[18] D. Maio, D. Maltoni, R. Cappelli, J. L. Wayman, and A. K. Jain, "FVC2004: Third fingerprint verification competition," in *Proc. 1st Int. Conf. Biometric Authentication (ICBA)*, 2004, pp. 1–7.

[19] M. S. M. Asaari, S. A. Suandi, and B. A. Rosdi, "Fusion of band limited phase only correlation and width centroid contour distance for finger based biometrics," *Expert Syst. Appl.*, vol. 41, no. 7, pp. 3367–3382, 2014.

[20] Y. Lu, S. J. Xie, S. Yoon, Z. Wang, and D. S. Park, "An available database for the research of finger vein recognition," in *Proc. 6th Int. Congr. Image Signal Process. (CISP)*, vol. 1, 2013, pp. 410–415.

[21] P. Tome, M. Vanoni, and S. Marcel, "On the vulnerability of finger vein recognition to spoofing," in *Proc. IEEE Int. Conf. Biometrics Special Interest Group (BIOSIG)*, Sep. 2014, pp. 1–10. [Online]. Available: http://publications.idiap.ch/index.php/publications/show/2910

[22] W. Yang, X. Yu, and Q. Liao, "Personal authentication using finger vein pattern and finger-dorsa texture fusion," in *Proc. 17th ACM Int. Conf. Multimedia*, 2009, pp. 905–908.

[23] L. Yang, G. Yang, Y. Yin, and R. Xiao, "Sliding window-based region of interest extraction for finger vein images," *Sensors*, vol. 13, no. 3, pp. 3799–3815, 2013.

Bernhard Prommegger received the M.Sc. degree in applied image and signal processing from the University of Salzburg and the University of Applied Sciences Salzburg in 2014 and the DI (Austrian equivalent to M.Sc.) degree in information technology and systems management from the University of Applied Sciences Salzburg in 2015. He is currently pursuing the Ph.D. degree in applied image and signal processing with the Department of Computer Sciences, University of Salzburg, where he is currently a Research Assistant. His main research interest is in vascular biometrics, especially multiperspective finger vein biometrics.

Christof Kauba received the B.Eng. and M.Sc. degrees and the Ph.D. degree in applied information technology from the University of Salzburg, Austria, in 2013, 2015, and 2018, respectively, where he is a Post-Doctoral Researcher with the Department of Computer Sciences. His research interests include image and video processing, image forensics and biometrics, especially biometric sensor design as well as finger- and hand-vein biometrics.

Michael Linortner received the DI (Austrian equivalent to M.Sc.) degree in information technology and systems management from the University of Applied Sciences Salzburg in 2017. He is currently a Research Assistant with the Department of Computer Sciences, University of Salzburg. His main research interest is in vascular biometrics, especially finger vein biometrics.

Andreas Uhl is a Professor with the Department of Computer Sciences, University of Salzburg, where he heads the Multimedia Processing and Security Lab. His research interests include image and video processing and compression, wavelets, media security, medical imaging, biometrics, and number-theoretical numerics.